NASA TECHNICAL NOTE

NASA TN D-8168

NASA TN D-8168

OPTIMAL THREE-DIMENSIONAL REUSABLE TUG TRAJECTORIES FOR PLANETARY MISSIONS INCLUDING CORRECTION FOR NODAL PRECESSION

Janos Borsody

Lewis Research Center

Cleveland, Ohio 44135

NATIONAL AERONAUTICS AND SPACE ADMINISTRATION • WASHINGTON, D. C. • FEBRUARY 1976

1 Report No	2 Government Accession No	3 Recipient's Catalog No
NASA TN D-8168		

4 Title and Subtitle	5 Report Date
OPTIMAL THREE-DIMENSIONAL REUSABLE TUG TRAJECTORIES FOR PLANETARY MISSIONS INCLUDING CORRECTION FOR NODAL PRECESSION	February 1976
	6 Performing Organization Code
7 Author(s)	8 Performing Organization Report No
Janos Borsody	E-8498
	10 Work Unit No
9 Performing Organization Name and Address	491-62
Lewis Research Center National Aeronautics and Space Administration Cleveland, Ohio 44135	11 Contract or Grant No
	13 Type of Report and Period Covered
12 Sponsoring Agency Name and Address	Technical Note
National Aeronautics and Space Administration Washington, D.C. 20546	14 Sponsoring Agency Code

15 Supplementary Notes

16 Abstract

Equations are derived by using the Maximum Principle to maximize the payload of a reusable Tug for planetary missions. The analysis includes a correction for precession of the Space Shuttle orbit. The Tug returns to this precessed orbit (within a specified time) and makes the required nodal correction. A sample case is analyzed that represents an inner-planet mission as specified by a fixed declination and right ascension of the outgoing asymptote and the mission energy. The reusable stage performance corresponds to that of a typical cryogenic Tug. Effects of Space Shuttle orbital inclination, several trajectory parameters, and Tug thrust on payload are also investigated.

17 Key Words (Suggested by Author(s))	18 Distribution Statement
Space flight Space rendezvous Space transportation Space Tugs	Unclassified - unlimited STAR Category 15 (rev)

19 Security Classif (of this report)	20 Security Classif (of this page)	21 No of Pages	22 Price*
Unclassified	Unclassified	42	$3.75

* For sale by the National Technical Information Service, Springfield Virginia 22161

OPTIMAL THREE-DIMENSIONAL REUSABLE TUG TRAJECTORIES FOR PLANETARY MISSIONS INCLUDING CORRECTION FOR NODAL PRECESSION

by Janos Borsody

Lewis Research Center

SUMMARY

Maximum payload capability for a reusable Tug is calculated by using the Maximum Principle to derive the equations governing the problem. The analysis includes a correction for precession of the Space Shuttle (SS) orbit. The two-point boundary value problem is solved by using finite difference partial derivatives and a Newton-Raphson iteration technique.

Data are presented for a given planetary mission and cryogenic Tug and include, in addition to payload capability, several trajectory parameters that are necessary to define the flight profile and the outgoing asymptote.

Inclination of the initial SS orbit is varied from 28.5° to 90° to show the effect of inclination on Tug performance. Other parameters varied are Tug thrust, total trip time, and payload-separation coast time. Total trip time is defined as the time between Tug departure from and return to the SS orbit. Payload-separation coast time is the time from the Tug outbound burn cutoff to retroburn start.

INTRODUCTION

At the present time the National Aeronautics and Space Administration (NASA) is developing a reusable Space Shuttle (SS). As it becomes operational, many unmanned missions will be launched with the SS. It will carry and directly deploy payloads to low Earth orbits. For high-Earth-orbits and planetary missions, however, an upper stage (carried in the SS cargo bay along with the payload) is required. One option available for performing these higher energy missions is to use an expendable stage in conjunction with the SS. To analyze the performance and launch availability of this configuration for planetary missions is relatively simple using methods already developed for expendable launch vehicles.

However, past NASA studies indicate that in order to reduce space transportation and payload costs, the SS upper stage should be reusable. This new, reusable stage is generally called a Tug. Performance analysis of the SS and Tug transportation system is far more complicated than when the expendable configuration is used, since the Tug must be returned to rendezvous with the SS for recovery and reuse.

This report presents a method for determining the maximum performance of a reusable SS upper stage for planetary missions and demonstrates this method by analyzing a particular stage for several sample cases. The mathematical formulation of the problem is three dimensional, and a two-point boundary value problem is derived by using the Maximum Principle.

Methods that have been used to determine reusable Tug performance for planetary missions are largely limited to ideal impulsive calculations and planar integrated trajectory simulations (refs. 1 and 2). These methods do not allow for a complete definition of planetary mission requirements, nor do they account for nodal precession.

The analysis presented in this report relaxes the planar constraint and allows out-of-plane thrusting. It also includes a complete definition of a planetary mission in terms of the declination and right ascension of the outgoing asymptote and the mission energy. The right ascension of the outgoing asymptote is not constrained in the analysis. However, with the information provided, the necessary right ascension can be satisfied by proper selection of SS launch time.

The flight profiles presented are designed to correct for nodal precession of the SS orbit during the mission. Nodal precession (nodal shift) is caused by the Earth's oblateness, which induces a retrograde motion of orbital planes about the polar axis. This rate of rotation is about 0.3 degree per hour for low Earth orbits. Since the time between Tug departure from and return to the SS orbit may be as long as 2 days, nodal shift becomes a major concern and a trajectory consideration.

The maximum payload capability of a representative Tug configuration is presented in this report for a range of declinations and a range of departure-orbit inclinations. The mission energy selected corresponds to a typical inner-planet delivery mission. Effects of total trip time, Tug initial thrust-to-weight ratio, and payload-separation coast time are also discussed.

ANALYSIS

Assumptions and Simplifications

A simplified trajectory and flight profile for the mission to be analyzed in this report is presented in sketch (a). It consists of an outbound burn, a retroburn, and apogee and perigee burns. At outbound burn completion, three conditions that define the outgoing

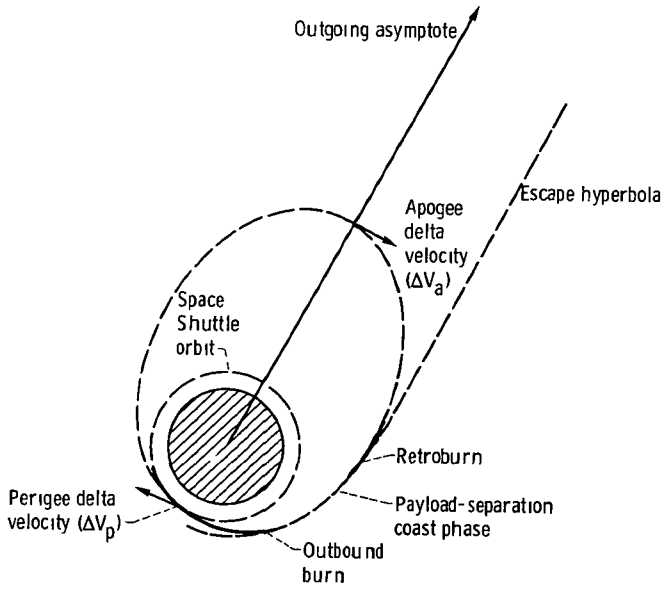

(a)

asymptote of the escape hyperbola for a planetary mission must be satisfied. They are the declination and right ascension of the outgoing asymptote and the mission energy. The outbound burn is terminated when the desired mission energy is reached. At this point the engine is shut down and payload separation is initiated.

During the fixed coast phase that follows engine shutdown, the payload is separated and the Tug is turned around for proper alinement to perform a retroburn. Since during retroburn the Tug engine is pointed toward the spacecraft, there is concern about exhaust impingement on the spacecraft. In order to avoid this problem, a separation velocity must be imparted to the spacecraft, and the coast phase must be long enough to allow for a safe separation distance between the Tug and the spacecraft. At the end of the payload-separation coast phase (fixed time from outbound-burn cutoff to retroburn start), a retroburn maneuver is performed that reduces hyperbolic excess velocity to subescape velocity and puts the Tug into an elliptic orbit. The length of this burn is primarily dependent on the given Tug trip time. Trip time is defined as the elapsed time from Tug outbound-burn ignition to return to the SS orbit. At the end of retroburn, the Tug is constrained to be in the same orbital plane that the SS will be in at rendezvous.

Retroburn is followed by a coast phase to the apogee of this intermediate Tug orbit, where a small delta velocity is added to adjust perigee altitude to correspond to the perigee altitude of the SS orbit. This velocity change is followed by a coast phase to perigee, where the apogee of this intermediate orbit is reduced to correspond with the apogee altitude of the SS orbit.

Since the SS remains in a low Earth orbit while the Tug delivers the spacecraft and returns to rendezvous with the SS, there is a substantial nodal shift and corresponding plane change between the SS orbit at Tug departure and the final SS rendezvous orbit. Nodal shift is caused by the Earth's oblateness. The added attraction of the equatorial bulge introduces a force normal to and toward the equatorial plane. The resultant acceleration will cause the SS to cross the equator before the point at which it would cross if a spherical Earth were assumed. This motion of the line of nodes is called nodal precession or nodal shift. Nodal precession is discussed in more detail in the following section. Since the SS does not have the performance capability to substantially change the line of nodes, the Tug must perform out-of-plane maneuvers to correct for nodal precession. In this report it is assumed that all nodal correction is done during the outbound burn and retroburn. Alternative approaches would be to introduce an additional nodal correction burn or to combine some nodal correction with the apogee and perigee burns. These alternative approaches were not evaluated, and it is not clear if they offer any theoretical improvements over the approach used in this report. Based on the results obtained, the added nodal correction burn, even if theoretically optimum, may not be justified, since the payload loss due to nodal correction is quite small (section RESULTS AND DISCUSSION). While small payload gains might be theoretically realized by the addition of a nodal correction burn, the losses associated with an additional start-up and shutdown could nullify these payload gains. In deriving the equations of motion governing the problem, the following assumptions were made:

(1) A spherical nonrotating Earth model is assumed. This implies that there is no nodal shift or apsidal precession of the intermediate Tug orbits. The Tug will correct for SS orbital precession only. This gives somewhat conservative Tug performance, since if the Tug orbits were allowed to precess, total nodal correction required would be slightly reduced and consequently payload capability would increase. For the mission analyzed herein, the nodal shift of intermediate Tug orbits is less than 2 percent of the nodal shift of the SS orbit. Although a spherical Earth model is assumed in order to simplify the equations, a nonspherical Earth model could easily be incorporated without a major change in the analysis.

(2) The return leg of the mission (apogee and perigee maneuvers) is done impulsively. This assumption neglects gravitational and thrust-to-weight losses encountered during these burns. Apogee burn is very short and these losses would be very small and have a negligible effect on payload. Perigee burn is longer; but by this time most of the propellant is expended and consequently thrust-to-weight ratio is high. Thus, the burn is relatively short and the losses should be very small. These burns could be integrated, but this would significantly increase the iteration size in solving the two-point boundary value problem and hence greatly increase the difficulty of obtaining solutions.

(3) The cryogenic Tug used herein has a constant thrust and specific impulse, although the analysis is formulated to accommodate a variable-thrust Tug.

(4) The SS is injected into a circular orbit with a given inclination and altitude. The Tug can depart from this orbit at any point that is determined to give maximum payload. A circular departure orbit is selected to simplify Tug and SS rendezvous. This is discussed in greater detail later.

(5) The right ascension of the outgoing asymptote is not constrained in the trajectory optimization. A "pseudo right ascension" is defined as the longitude of the projection of the outgoing asymptote in the equatorial plane measured from the ascending node of the SS orbit. The true right ascension, then, is the sum of the pseudo right ascension and the longitude of the ascending node of the SS orbit as measured from the vernal equinox. This longitude may be varied by varying SS launch time. Hence, for a given pseudo right ascension, any desired right ascension of the outgoing asymptote may be obtained by selecting the proper SS launch time. Therefore, in this report an optimum pseudo right ascension is determined for each declination of the outgoing asymptote, and the right ascension requirements are assumed to be satisfied by selection of SS launch time.

If any unaccounted-for delay is encountered after the Tug is deployed in orbit, achieving the correct right ascension and declination becomes an important constraint in determining a Tug "launch window." This problem is not analyzed in this report.

(6) The analysis is done for a two-body problem, and all trajectory perturbations due to the Sun, Moon, and other planets are neglected.

Nodal and Apsidal Precession

Nodal precession has been analyzed and discussed in reference 3. An analytical expression of secular nodal shift using first-order expansion in the dominant oblateness parameter J is given by the following equation:

$$\Delta\Omega = -\frac{JG^{1/2}}{R_E^{3/2}} T_D \left(\frac{R_E}{p}\right)^{7/2} \left(1 - e^2\right)^{3/2} \cos i \qquad (1)$$

(Symbols and notation used are defined in appendix A.) Nodal precession is a function of orbital inclination, eccentricity, and semilatus rectum. It also depends on the length of time spent in orbit T_D (in this case total trip time), the equatorial radius and gravitational constant of the Earth, and the coefficient of the second harmonic J in the gravitational potential function. Equation (1) is used in this analysis to compute nodal precession for a given mission.

The line of apsides also advances on the celestial sphere as noted in reference 1. An analytical expression for this motion is given in terms of the change in argument of perigee as follows:

$$\Delta\omega = \frac{JG^{1/2}}{2R_E^{3/2}} T_D \left(\frac{R_E}{p}\right)^{7/2} \left(1 - e^2\right)^{3/2} (4 - 5 \sin^2 i) \tag{2}$$

This apsidal motion becomes very important if elliptic SS orbits are used, since proper apsidal orientation must be achieved between the Tug and SS orbits. For circular orbits, the apsidal precession translates into an effective reduction in the period of the SS orbit. However, this can easily be taken care of with minor payload loss or gain by varying the total trip time a few minutes. Although, theoretically, proper phasing of Tug and SS can be achieved by varying the total trip time, the operational aspects of this approach on Tug guidance hardware, software, and mission design requirements must be carefully evaluated. However, this is outside the scope of this report and is not discussed further. For simplicity a circular SS orbit is assumed in this report.

Basic Equations Governing the Problem

Equations governing the flight of a rocket in an inverse-square gravitational field are given by

$$\dot{\bar{V}} = -\frac{G}{r^3}\bar{r} + \frac{V_e \beta(\zeta)}{m}\hat{f} \tag{3}$$

$$\dot{\bar{r}} = \bar{V} \tag{4}$$

$$\dot{m} = -\beta(\zeta) \tag{5}$$

$$\dot{\zeta} = 1 \tag{6}$$

$$\hat{f} \cdot \hat{f} - 1 = 0 \tag{7}$$

In these equations, r, V, and m represent instantaneous radius, velocity, and mass, respectively; V_e is the engine exhaust velocity; β is the mass flow rate, which may be a function of time; and $\hat{f}$ is the unit thrust direction, which must be determined. The superscripts $-$ and $\hat{}$ represent vector and unit vector quantities, respectively; and $\cdot$ represents a derivative of the particular variable with respect to time. State variable ζ was introduced to remove the explicit time dependence of mass flow rate from the equation. This is standard procedure.

By using a Hamiltonian formulation of the Maximum Principle (ref. 4), the costate

equations may be obtained from the so-called Hamiltonian given by

$$H = \bar{\lambda} \cdot \dot{\bar{V}} + \bar{\mu} \cdot \dot{\bar{r}} + \sigma \dot{m} + \tau \dot{\zeta} + \gamma(\hat{f} \cdot \hat{f} - 1) \tag{8}$$

In this equation, $\bar{\lambda}$, $\bar{\mu}$, and σ are the adjoint variables associated with state variables $\bar{V}$, $\bar{r}$, and m and τ is associated with dummy variable ζ. The constraint associated with the thrust direction is also adjoined to H by γ. From equation (8) the time derivatives of the adjoint variables are given by

$$\dot{\bar{\lambda}} = -\bar{\mu} \tag{9}$$

$$\dot{\bar{\mu}} = \frac{G}{r^3}\left[\bar{\lambda} - 3\,(\bar{\lambda} \cdot \hat{r})\hat{r}\right] \tag{10}$$

$$\dot{\sigma} = \frac{V_e \beta}{m^2}(\bar{\lambda} \cdot \hat{f}) \tag{11}$$

$$\dot{\tau} = -K \frac{\partial \beta}{\partial \zeta} \tag{12}$$

where

$$K = \frac{V_e}{m}(\bar{\lambda} \cdot \hat{f}) - \sigma \tag{13}$$

The thrust direction that minimizes the Hamiltonian is given by

$$\hat{f} = \hat{\lambda} \tag{14}$$

and

$$\gamma = -\frac{V_e \beta}{2m}\lambda \tag{15}$$

State equations (3) to (6) and adjoint equations (9) to (12) make up a set of first-order nonlinear differential equations which must be numerically integrated in order to obtain a solution to the two-point boundary value problem. Optimum thrust direction is along the unit λ vector given by equation (14).

Trajectory Constraints

In this section, constraints on the problem are discussed in more detail. Sketch (b) illustrates a simplified trajectory profile departing from a given initial orbit. Events a_i

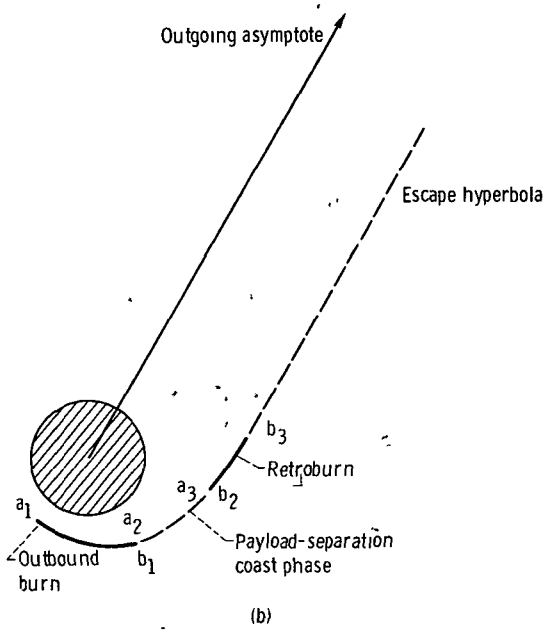

(b)

and b_i (i = 1 to 3) are also indicated on the sketch. The outbound burn is initiated at time $a_1 = 0$ at an optimal point in the initial circular inclined orbit. Thrust is terminated when the desired mission energy is reached. This is followed by a given coast phase until time b_2. At time a_3 ($a_3 = b_2$) a retroburn is initiated until time b_3 is reached, followed by the apogee and perigee delta-velocity maneuvers. It may already be obvious that a_i represents the time at the beginning of phase i and b_i is the time at phase i completion. With this convention, constraints governing the problem can be written mathematically as follows:

$$q_1 = r(a_1) - r_1 = 0 \tag{16a}$$

$$q_2 = V(a_1) - V_1 = 0 \tag{16b}$$

$$q_3 = \bar{r}(a_1) \cdot \bar{V}(a_1) = 0 \tag{16c}$$

$$q_4 = \hat{h}(a_1) \cdot \hat{i}_3 - \cos i_1 = 0 \tag{16d}$$

$$q_5 = -\hat{h}(a_1) \cdot \hat{\imath}_2 - \cos \Omega_1 \sin i_1 = 0 \tag{16e}$$

$$q_6 = m(a_1) - m_1 = 0 \tag{16f}$$

$$\bar{q}_7 = \bar{r}(a_3) - \bar{r}(b_2) = \bar{0} \tag{16g}$$

$$\bar{q}_8 = \bar{V}(a_3) - \bar{V}(b_2) = \bar{0} \tag{16h}$$

$$q_9 = E\left[r(b_2), V(b_2)\right] - E_D = 0 \tag{16i}$$

$$q_{10} = \varphi\left[r(b_2), V(b_2)\right] - \varphi_D = 0 \tag{16j}$$

$$q_{11} = m(b_3) - m_H e^{1/V_e(\Delta V_a + \Delta V_p)} = 0 \tag{16k}$$

$$q_{12} = \hat{r}(b_3) \cdot \hat{h}_o = 0 \tag{16l}$$

$$q_{13} = \hat{V}(b_3) \cdot \hat{h}_o = 0 \tag{16m}$$

$$q_{14} = b_3 - a_1 + T - T_D = 0 \tag{16n}$$

$$q_{15} = a_3 - b_2 = 0 \tag{16o}$$

$$\bar{q}_{16} = \bar{r}(a_2) - \bar{r}(b_1) = \bar{0} \tag{16p}$$

$$\bar{q}_{17} = \bar{V}(a_2) - \bar{V}(b_1) = \bar{0} \tag{16q}$$

$$q_{18} = a_2 + \Delta t - b_2 = 0 \tag{16r}$$

$$q_{19} = a_2 - b_1 = 0 \tag{16s}$$

$$q_{20} = m(a_2) - m(b_1) = 0 \tag{16t}$$

Equations (16a) to (16f) express fixed initial conditions, while (16g) and (16h) express the continuity of position and velocity vectors at injection. Equation (16i) gives a fixed energy requirement. Equation (16j) is the constraint for fixed declination of the outgoing asymptote, (16k) is the constraint on Tug mass required at b_3 to perform the apogee and perigee delta velocity maneuvers and return the Tug empty to the rendezvous orbit. The term $\hat{h}_o$ in equations (16ℓ) and (16m) is the unit angular momentum vector of the precessed SS orbit to which the Tug must return. These constraints assure that the Tug will be in the proper orbit for rendezvous at the end of retroburn. Equation (16n) expresses the total-trip-time constraint associated with the problem. Equations (16p) to (16t) express the constraints at the beginning of payload separation.

With these constraints, the augmented Hamiltonian to be minimized can be written as follows:

$$H^* = m(a_3) - m(b_2) + \sum_{i=1}^{3} H_i + \sum_{i=1}^{20} \epsilon_i q_i$$

The absolute value of $m(a_3) - m(b_2)$ represents payload dropped during the coast phase. The term H_i represents the Hamiltonians during outbound burn, payload-separation coast phase, and retroburn. Constraints q_i are adjoined to H^* by using the arbitrary multipliers ϵ. Auxiliary variational conditions associated with the two-point boundary value problem can be derived by using this augmented Hamiltonian.

Auxiliary Variational Equations

By using the Hamiltonian Maximum Principle (ref. 5) and the constraints described in the previous section, the following auxiliary variational equations must be satisfied to maximize payload:

$$\bar{\lambda}(a_1) = \epsilon_2 \hat{\bar{V}}(a_1) + \epsilon_3 \bar{r}(a_1) + \epsilon_4 \nabla_{\bar{V}} q_4 + \epsilon_5 \nabla_{\bar{r}} q_5 \tag{17a}$$

$$\bar{\mu}(a_1) = \epsilon_1 \hat{\bar{r}}(a_1) + \epsilon_3 \bar{V}(a_1) + \epsilon_4 \nabla_{\bar{r}} q_4 + \epsilon_5 \nabla_{\bar{r}} q_5 \tag{17b}$$

$$\bar{\lambda}(a_2) = \bar{\lambda}(b_1) \tag{17c}$$

$$\bar{\mu}(a_2) = \bar{\mu}(b_1) \tag{17d}$$

$$\sigma(a_2) = \sigma(b_1) \tag{17e}$$

$$\bar{\lambda}(a_3) = \bar{\lambda}(b_2) + \epsilon_9 \bar{V}(b_2) + \epsilon_{10} \nabla_{\bar{V}} \varphi \tag{17f}$$

$$\bar{\mu}(a_3) = \bar{\mu}(b_2) + \epsilon_9 \frac{G}{r^3} \bar{r}(b_2) + \epsilon_{10} \nabla_{\bar{r}} \varphi \tag{17g}$$

$$\sigma(a_3) = 1 \tag{17h}$$

$$\sigma(b_2) = 1 \tag{17i}$$

$$\bar{\lambda}(b_3) + \left[H(b_3) - \tau(b_3)\right] \nabla_{\bar{V}} T + \sigma(b_3) \frac{m(b_3)}{V_e} \nabla_{\bar{V}} \Delta V_T + \frac{\epsilon_{13}}{V(b_3)} \left[\hat{h}_o - \hat{h}_o \cdot \hat{V}(b_3) \hat{V}(b_3)\right] = \bar{0} \tag{17j}$$

$$\bar{\mu}(b_3) + \left[H(b_3) - \tau(b_3)\right] \nabla_{\bar{r}} T + \sigma(b_3) \frac{m(b_3)}{V_e} \nabla_{\bar{r}} \Delta V_T + \frac{\epsilon_{12}}{r(b_3)} \left[\hat{h}_o - \hat{h}_o \cdot \hat{r}(b_3) \hat{r}(b_3)\right] = \bar{0} \tag{17k}$$

$$\left[H(a_2) - \tau(a_2)\right] - \left[H(b_1) - \tau(b_1)\right] + \left[H(a_3) - \tau(a_3)\right] - \left[H(b_2) - \tau(b_2)\right] = 0 \tag{17l}$$

In these equations, ϵ_i represents arbitrary constants. Equations (17c) to (17e) express the continuity of adjoint variables at the beginning of the payload-separation coast phase, and (17f) and (17g) give the discontinuity in $\bar{\lambda}$ and $\bar{\mu}$ at the end of this coast phase. The multiplier σ associated with mass is continuous and is equal to 1 at the end of the coast phase. Equations (17j) and (17k) must be satisfied at the end of retroburn for maximum payload. Gradients of return time T, total delta velocity ($\Delta V_T = \Delta V_a + \Delta V_p$), and declination φ are derived in appendixes B, C, and D, respectively. Return time is defined as the time from retroburn completion to rendezvous with the SS.

Evaluation of Discontinuity in State Variables at the End of Payload-Separation Coast Phase

In order to determine the discontinuity in $\bar{\lambda}$ and $\bar{\mu}$ at time a_2, two arbitrary constants (ϵ_9 and ϵ_{10}) must be evaluated in equations (17f) and (17g). First, the arbitrary

constant ϵ_{10} is evaluated as follows:
Let

$$\bar{C}(t) = \bar{\lambda}(t) \times \bar{V}(t) + \bar{\mu}(t) \times \bar{r}(t) \tag{18}$$

where $\times$ represents cross product of two vectors and vector $\bar{C}$ is a constant of motion ($C(t)$ = constant vector). This can be shown by taking the time derivative of $\bar{C}$ and substituting equations (3), (4), (9), and (10) for $\dot{\bar{V}}$, $\dot{\bar{r}}$, $\dot{\bar{\lambda}}$, and $\dot{\bar{\mu}}$, respectively. The time derivative is identically zero; therefore, $\bar{C}$ is a constant of motion. Taking the cross product of equation (17f) with $\bar{V}$ and (17g) with $\bar{r}$ gives

$$\bar{C}(a_3) - \bar{C}(b_2) = \epsilon_{10} \left[\nabla_{\bar{V}} \varphi \times \bar{V}(b_2) + \nabla_{\bar{r}} \varphi \times \bar{r}(b_2) \right] \tag{19}$$

The constancy of $\bar{C}$ during retroburn implies that

$$\bar{C}(a_3) = \bar{C}(b_3) \tag{20}$$

Using equations (17j) and (17k) gives

$$\bar{C}(b_3) = -\hat{h}_o \times \left[\epsilon_{13} \hat{V}(b_3) + \epsilon_{12} \hat{r}(b_3) \right] \tag{21}$$

This equation was derived by using the results of reference 6, where it is shown that $\nabla_{\bar{V}} y \times \bar{V} + \nabla_{\bar{r}} y \times \bar{r} = \bar{0}$ if $y = y\left[r, V, \bar{r} \cdot \bar{V}\right]$. Since return time and apogee and perigee delta velocities are of this form, the corresponding cross products are zero. From equation (21) it is obvious that

$$\bar{C}(b_3) \cdot \hat{h}_o = 0 \tag{22}$$

Taking the dot product of equation (19) with $\hat{h}_o$, substituting equation (22), and solving for ϵ_{10} give

$$\epsilon_{10} = \frac{\bar{C}(b_2) \cdot \hat{h}_o}{\left[\nabla_{\bar{V}} \varphi \times \bar{V}(b_2) + \nabla_{\bar{r}} \varphi \times \bar{r}(b_2) \right] \cdot \hat{h}_o} \tag{23}$$

Given ϵ_{10} and $\lambda(b_2)$, let

$$\bar{X} = \bar{\lambda}(b_2) + \epsilon_{10} \nabla_{\bar{V}} \varphi \tag{24}$$

With this definition, equation (17f) becomes

$$\bar{\lambda}(a_3) = \epsilon_9 \bar{V}(b_2) + \bar{X} \tag{25}$$

In order to determine the discontinuity in $\bar{\lambda}$ and $\bar{\mu}$, ϵ_9 must also be evaluated. This may be done as follows: Substitute equations (17c), (17d), (17f), and (17g) into equation (17ℓ), which gives

$$\beta(a_3)\left[\frac{V_e\lambda(a_3)}{m(a_3)} - \sigma(a_3)\right] - \beta(b_1)\left[\frac{V_e\lambda(b_1)}{m(b_1)} - \sigma(b_1)\right] = 0 \tag{26}$$

Since $\beta(a_3) = \beta(b_1) \neq 0$, equation (26) can be divided by $\beta(a_3)$. Also $\dot{\sigma} = 0$ during a coast phase (σ is constant); therefore, equations (17e), (17h), and (17i) give $\sigma(a_3) = \sigma(b_1)$ and equation (26) reduces to

$$\lambda(a_3) = \frac{m(a_3)}{m(b_1)}\lambda(b_1) \tag{27}$$

Substituting equation (27) into (25) and solving for ϵ_9 give

$$\epsilon_9 = -\frac{1}{V(b_2)}\left\{\bar{X}\cdot\hat{V}(b_2) \pm \sqrt{\left[\bar{X}\cdot\hat{V}(b_2)\right]^2 + \left[\frac{m(a_3)\lambda(b_1)}{m(b_1)}\right]^2 - X^2}\right\} \tag{28}$$

The choice of + or - sign can be determined as follows: Assume the payload is zero; that is, $m(a_3) = m(b_1)$. Also if the declination is not specified, equation (24) becomes $\bar{X} = \bar{\lambda}(b_2)$. Furthermore, if the coast phase is zero, $\lambda(b_2) = \lambda(b_1)$. With these assumptions, equation (28) becomes

$$\epsilon_9 = -\frac{1}{V(b_2)}\left[\bar{\lambda}(b_2)\cdot\hat{V}(b_2) \pm \bar{\lambda}(b_2)\cdot\hat{V}(b_2)\right]$$

A choice of - sign implies that $\epsilon_9 = 0$ and that the thrust direction is continuous at a_3, essentially pointed along the velocity vector. However, in order to bring the Tug back, the velocity must be reduced to below escape velocity, and the thrust direction should be opposite to the velocity vector. Therefore the + sign should be used in equation (28).

Variational Final Conditions at Termination of Retroburn

In this section, final conditions at the termination of retroburn are derived. Substituting equations (17j) and (17k) into equation (8) gives

$$\left[H(b_3) - \pi(b_3)\right]\left[1 - \frac{G}{r^3(b_3)} \nabla_{\bar{V}} T \cdot \bar{r}(b_3) + \nabla_{\bar{r}} T \cdot \bar{V}(b_3)\right] =$$

$$- \sigma(b_3) \frac{m(b_3)}{V_e}\left[- \frac{G}{r^3(b_3)} \nabla_{\bar{V}} \Delta V_T \cdot \bar{r}(b_3) + \nabla_{\bar{r}} \Delta V_T \cdot \bar{V}(b_3)\right]$$

$$+ \beta(b_3)\left[\frac{V_e \lambda(b_3)}{m(b_3)} - \sigma(b_3)\right] \tag{29}$$

However,

$$- \frac{G}{r^3(b_3)} \nabla_{\bar{V}} T \cdot \bar{r}(b_3) + \nabla_{\bar{r}} T \cdot \bar{V}(b_3) = \frac{dT}{dt}$$

and

$$- \frac{G}{r^3(b_3)} \nabla_{\bar{V}} \Delta V_T \cdot \bar{r}(b_3) + \nabla_{\bar{r}} \Delta V_T \cdot \bar{V}(b_3) = \frac{d\,\Delta V_T}{dt}$$

These equations are valid for a coast phase ($\beta = 0$). However, the total delta velocity required to return the Tug does not change during a coast phase, and $d\,\Delta V_T/dt = 0$. Similarly, the change in return time is equal to the change in time along the coast arc but opposite in sign; that is, $dT/dt = -1$. Substitution of these results into equation (29) gives

$$\sigma(b_3) = \frac{V_e \lambda(b_3)}{m(b_3)} \tag{30}$$

The arbitrary constants ϵ_{12} and ϵ_{13} in equations (17j) and (17k) can be evaluated by taking the dot product of equation (21) with $\bar{r}(b_3)$ and $\bar{V}(b_3)$:

$$\frac{\epsilon_{13}}{V(b_3)} = -\frac{\bar{\lambda}(b_3)\cdot\hat{h}(b_3)}{\hat{h}(b_3)\cdot\hat{h}_o} \tag{31}$$

and

$$\frac{\epsilon_{12}}{r(b_3)} = -\frac{\bar{\mu}(b_3)\cdot\hat{h}(b_3)}{\hat{h}(b_3)\cdot\hat{h}_o} \tag{32}$$

The remaining two variational conditions can be obtained by taking the dot product of equation (17j) with $\nabla_{\bar{V}}\,\Delta V_T$ and (17k) with $\nabla_{\bar{r}}\,\Delta V_T$:

$$\left\{\bar{\lambda}(b_3) - \lambda(b_3)\nabla_{\bar{V}}\,\Delta V_T + \left[H(b_3) - \tau(b_3)\right]\nabla_{\bar{V}}T - \frac{\bar{\lambda}(b_3)\cdot\hat{h}(b_3)}{\hat{h}(b_3)\cdot\hat{h}_o}\left[\hat{h}_o - \hat{h}_o\cdot\hat{V}(b_3)\hat{V}(b_3)\right]\right\}\cdot\nabla_{\bar{V}}\,\Delta V_T = 0 \tag{33}$$

$$\left\{\bar{\mu}(b_3) + \lambda(b_3)\nabla_{\bar{r}}\,\Delta V_T + \left[H(b_3) - \tau(b_3)\right]\nabla_{\bar{r}}T - \frac{\bar{\mu}(b_3)\cdot\hat{h}(b_3)}{\hat{h}(b_3)\cdot\hat{h}_o}\left[\hat{h}_o - \hat{h}_o\cdot\hat{r}(b_3)\hat{r}(b_3)\right]\right\}\cdot\nabla_{\bar{r}}\,\Delta V_T = 0 \tag{34}$$

where

$$H(b_3) - \tau(b_3) = -\frac{G}{r^3(b_3)}\,\bar{\lambda}(b_3)\cdot\bar{r}(b_3) + \bar{\mu}(b_3)\cdot\bar{V}(b_3) \tag{35}$$

Equations (33) and (34) must be satisfied by the solution of the two-point boundary value problem. In order to assure this, they will be used as final conditions to be satisfied during the Newton-Raphson iteration.

Variational Final Condition at Departure from Initial Orbit

Equations (17a) and (17b) are six equations with five arbitrary constants. This implies there is a variational equation that must be satisfied. The variational condition may be obtained by computing the $\bar{C}$ vector at a_1:

$$\bar{C}(a_1) = (\epsilon_4 \hat{l}_3 - \epsilon_5 \hat{l}_2) \times \hat{h}(a_1) \tag{36}$$

From this equation the variational final condition is obtained by taking the dot product with $\hat{h}(a_1)$:

$$\bar{C}(a_1) \cdot \hat{h}(a_1) = 0 \tag{37}$$

Initial and Final Conditions

The initial adjoint variables are unknown and must be guessed in solving the two-point boundary value problem. As it is shown in reference 7, these variables can be replaced by physically more meaningful parameters, such as vehicle pitch attitude ψ, pitch rate $\dot{\psi}$, yaw attitude δ, yaw rate $\dot{\delta}$, and $\lambda(a_1)$ and $\dot{\lambda}(a_1)$ instead of the components of $\bar{\lambda}(a_1)$ and $\bar{\mu}(a_1)$. With these changes in variables, the free initial conditions and associated final conditions are as follows:

Initial conditions	Final conditions	
$\psi(a_1)$	$\hat{r}(b_3) \cdot \hat{h}_o = 0$	(38a)
$\dot{\psi}(a_1)$	$\hat{V}(b_3) \cdot \hat{h}_o = 0$	(38b)
$\delta(a_1)$	$\varphi\left[r(b_2), V(b_2)\right] - \varphi_D = 0$	(38c)
$\dot{\delta}(a_1)$	Equation (33)	(38d)
$\lambda(a_1)$	$\sigma(a_3) = \sigma(b_2) = 1$	(38e)
$\dot{\lambda}(a_1)$	$\bar{C}(a_1) \cdot \hat{h}(a_1) = 0$	(38f)
b_1	$E\left[r(b_2), V(b_2)\right] - E_D = 0$	(38g)
b_3	$b_3 - a_1 + T - T_D = 0$	(38h)
$m_p = m(a_3) - m(b_2)$	$m(b_3) - m_H e^{\Delta V_T / V_e} = 0$	(38i)
$u(a_1)$	Equation (34)	(38j)

Condition (38e) can be omitted from the iteration since the entire problem can be scaled by $\lambda(a_1)$, and this condition is satisfied by scaling the problem. Conditions (38g) and (38h) are removed from the iteration by initiating the payload-separation coast phase when the desired energy is reached and terminating the retroburn when the desired total trip time is satisfied. These two conditions are used as cutoff variables during the iteration. Final condition (38f) is used to compute $\dot{\lambda}(a_1)$, as shown in reference 5. With these simplifications, the number of final conditions to be satisfied is reduced to six, namely, equations (38a) to (38d), (38i), and (38j).

In order to solve the two-point boundary value problem, a finite difference Newton-Raphson iteration technique is used. The iteration is terminated when the percentage of predicted payload change and the absolute value of the normalized desired final conditions are less than 10^{-5}.

RESULTS AND DISCUSSION

The method described in the previous sections was applied to a typical cryogenic Tug configuration for a specific set of planetary target conditions. The results of that analysis are presented in this section. Performance and weight data for the Tug configuration are given in table I. Specific impulse has been reduced by 2 percent to account for flight performance reserves. Engine specific impulse corresponds to an uprated version of the current Centaur RL-10 engine. Combined weight of the Tug and payload is assumed to be constant (28 622 kg) and consistent with SS payload weight capability. Tug propellant load is varied to maintain this fixed initial weight. The baseline mission characteristics are presented in table II. Tug departure orbit is a 185-kilometer-altitude circular orbit inclined 28.5°. The Tug is free to depart from this orbit at any point. The departure point is chosen to maximize the injected payload.

Planetary missions most often are defined by specifying the mission energy and the right ascension and declination of the outgoing asymptote. The right ascension for a specific mission can be satisfied by selecting the proper SS launch time, as discussed earlier. Therefore, this constraint was not included in the analysis, and an optimum pseudo right ascension was obtained for each declination. Declination of the outgoing asymptote (often referred to as DLA) is parametrically varied from -40° to $+40^{\circ}$. A mission energy of 12 km^2/sec^2 was selected as a representative energy typical of an inner-planet (Mars and/or Venus) mission. Total Tug trip time for the baseline mission is 1 day, and payload-separation coast time is assumed to be 10 minutes.

Space Shuttle orbital inclination, total trip time, payload-separation coast time, and engine thrust are examined later in this section to determine their effects on Tug performance.

In order to explain the results that follow, it is helpful to recall some well-known facts from orbital geometry and previous analyses of planetary missions for expendable stages. If the nodal precession of the SS orbit is assumed to be zero and a spherical Earth model and planar trajectories are used (no nodal precession during the flight), for a fixed initial SS orbit, the same optimum payload can be delivered to all DLA's whose absolute value is less than the initial SS orbital inclination. Also there are two distinct solutions for each DLA whose absolute value is less than the SS orbital inclination. As the DLA approaches SS orbital inclination, the two solutions tend to coincide. At a DLA equal to SS orbital inclination, they degenerate into a single solution. DLA's whose absolute value is greater than SS orbital inclination can be reached only if yaw maneuvers are performed to increase inclination to or beyond the absolute value of the desired DLA. These yaw maneuvers reduce performance rapidly. Therefore, for these high DLA's, maximum performance is obtained when the orbital inclination is equal to the absolute value of the DLA; and there is a single solution for each DLA.

When nodal correction associated with the present problem is included, small plane-change maneuvers must be performed to correct for SS orbital precession. This will reduce Tug performance, but it should not substantially affect the orbital geometry. It is expected that there will be two solutions for DLA's whose absolute value is less than the SS orbital inclination and a single solution for DLA's whose absolute value is greater than the SS orbital inclination.

Another important point to recall is that the rates of change of the orbital inclination and the longitude of the line of nodes vary sinusoidally with orbital position for a fixed out-of-plane acceleration. The rate of change of the orbital inclination is maximum when the out-of-plane acceleration is applied at the line of nodes. The maximum change in the longitude of the line of nodes occurs when acceleration is applied at the antinode. This implies that, for a fixed amount of propellant expended, the maximum inclination change is obtained when the burn is at or near the line of nodes and the maximum change in the longitude of the line of nodes is obtained when the burn is added at or near the antinode. It is also important to note that an out-of-plane acceleration that tends to increase inclination near the line of nodes will move the line of nodes retrograde when applied ahead of the node and posigrade applied past the line of nodes. Since the line of nodes for the present problem must be moved retrograde approximately 8^{o}, for the DLA's where the outbound burn traverses the line of nodes, nodal shift during this burn is expected to be small.

Results obtained for the baseline Tug and baseline mission are presented in figures 1 to 6 as a function of DLA. Three SS orbital inclinations were analyzed: 28.5^{o}, 33.5^{o}, and 38.5^{o}. The minimum inclination that can be reached with a planar SS launch from the Eastern Test Range is 28.5^{o}. Since the SS does not have substantial dogleg capability, lower inclinations were not evaluated.

Figure 1 gives optimum pseudo right ascension as a function of DLA. As is explained in an earlier section, Assumptions and Simplifications, pseudo right ascension permits the user of the data to satisfy specific requirements on the right ascension of the outgoing asymptote by selecting SS launch time. By subtracting the value of pseudo right ascension for the desired DLA from the required right ascension, the longitude of the ascending node for the SS orbit may be determined. Since the longitude of the ascending node for a given SS orbital inclination moves through 360^{o} every day, the needed longitude of the ascending node may be obtained simply by selecting the correct SS launch time. It was mentioned earlier that the SS deploys the Tug and payload into a low Earth orbit and that the Tug is free to depart from this orbit at any point. The point of departure was determined in solving the two-point boundary value problem; it is presented in figure 2 as a function of DLA. The Tug departure argument of latitude is defined as the angle measured in the initial SS orbital plane relative to the ascending node of this orbit. Positive argument of latitude implies that the Tug departs from the SS orbit past nodal passage. The shape of the escape hyperbola is determined by perigee radius, which changes little with DLA, and by mission energy, which is constant. Therefore, once a trajectory is optimized for a given DLA, the shape of the escape hyperbola does not change significantly as DLA is varied. As DLA is changed, the plane containing the escape hyperbola is essentially rotated about the angular momentum vector of the initial SS orbit until the correct geometry is obtained.

As the value of DLA is varied between the negative and positive values of SS orbital inclination, the argument of latitude and pseudo right ascension sweep through nearly a 180^{o} arc. Recall the earlier discussion on the existence of two distinct families of solutions for DLA's whose absolute value is less than SS orbital inclination. Figures 1 and 2 show only one family. The remaining family of solutions covers the remaining 180^{o} in argument of latitude and pseudo right ascension. The existence of these solutions was demonstrated numerically by taking the converged initial conditions for a given DLA, changing the signs of initial yaw attitude and yaw rate, and adding 180^{o} to the departure argument of latitude. With these initial conditions, the trajectory was integrated and without any iteration yielded a converged case satisfying all necessary boundary conditions for a DLA of the same magnitude but opposite sign. The pseudo right ascension for these solutions is equal to the pseudo right ascension obtained for the first solution plus 180^{o}. The nodal correction during outbound burn, orbital inclination at injection, Tug payload, and delta-velocity losses associated with the second family of solutions are mirror images of the first family about a DLA of 0^{o}. Since the second family of solutions can be obtained by using the data presented and following the preceding discussion, they are not given herein to avoid confusion.

Figure 3 shows the variation of orbital inclination at payload separation; figure 4 presents the change in the longitude of the ascending node during outbound burn. In the following discussion, figures 2 to 4 and the preceding discussion on changing line of

nodes and orbital inclination are used to explain the observed trajectory characteristics for the range of DLA's considered. For high negative DLA's, the outbound burn starts well past the line of nodes, at about 80° argument of latitude (fig. 2). The outbound burn arc for the baseline Tug and mission is about 100°. Therefore, the Tug burns through maximum latitude, which is an optimal region for changing the longitude of the line of nodes. Almost all nodal change is done during this burn (fig. 4).

Notice that the nodal change during the outbound burn decreases for those negative DLA's whose absolute value is greater than the SS orbital inclination. In order to reach these DLA's, orbital inclination must be increased beyond the initial SS orbital inclination (fig. 3). Since the Tug must return to the SS orbit, the same inclination change must be made during retroburn, and it becomes more efficient to perform a larger nodal shift during this burn. As DLA is increased, the outbound burn moves closer to the line of nodes (fig. 2); it becomes less efficient to change the longitude of the line of nodes; and nodal change decreases. Also, to move the node retrograde for these cases, the SS orbital inclination must be decreased (fig. 3). For DLA's between 0° and 16°, the outbound burn traverses the line of nodes, and nodal change for these cases during outbound burn is quite small (fig. 4), as expected. As DLA is further increased, the outbound burn begins well ahead of the node and nodal change increases. Also, SS orbital inclination increases (fig. 3) and moves the node in a retrograde direction. For DLA's larger than the initial SS orbital inclination, the inclination during the outbound burn must be increased. And again nodal change becomes more efficient during retroburn. The sharp corners on the curves for DLA's nearly equal to the SS orbital inclination in figures 3 and 4 correspond to the DLA's where the two solutions degenerate into a single solution. The reason these corners do not occur exactly at DLA's equal to the initial SS orbital inclination is that orbital inclination has been changed during the outbound burn to correct for nodal precession.

In figure 5, Tug payload capability is plotted as a function of DLA. Payload is maximum at a DLA of approximately 8° for the three inclinations, and any DLA between -30° and 30° can be reached with less than a 100-kilogram payload loss. Notice the rapid payload loss as DLA is increased beyond the initial SS orbital inclination. This loss is caused by the large inclination change required during outbound Tug burn to reach a given DLA (fig. 3) and by the requirement that the Tug return to the SS orbital inclination. The inclination change during retroburn must be equal and opposite to the inclination change made during outbound burn. Therefore, for a 1-degree increase in DLA, a minimum of 2 degrees inclination change must be made. This, of course, becomes very expensive in terms of Tug performance. Similarly, the payload is expected to decrease rapidly for high negative DLA's; however, because of numerical sensitivities encountered in the Newton-Raphson iteration technique, solutions for these declinations were not obtained. For these high negative DLA's, there is only a single solution; therefore,

the performance should be equal to that obtained for the positive DLA's. If all the solutions were plotted, the payload curves would be symmetric about a DLA of 0°.

Figure 6 gives delta-velocity loss as a function of DLA for the three SS orbital inclinations. Velocity loss is defined as the velocity required above ideal impulsive velocity. Ideal impulsive velocity is defined as the velocity needed above circular orbital velocity at a 185-kilometer altitude in order to reach a given energy. This loss is the result of finite thrust level, thrusting along nonoptimal portions of the trajectory, nodal shift change, trip time, and fixed payload-separation coast time. Total velocity loss presented is the sum of losses during outbound and inbound portions of the trajectory, and it remains relatively constant throughout the range of DLA's. At the limiting DLA's, both outbound and inbound velocity losses tend to increase sharply, resulting in a rapid decrease in payload capability. In order to show the delta-velocity loss due to nodal correction, velocity losses for a 90° initial SS orbital inclination (nodal precession of zero) are also presented. These cases are discussed later in this section. Notice that without nodal correction, the velocity losses remain constant. Velocity loss due to nodal shift for DLA's between -28° and 28° for an initial SS orbital inclination of 28.5° is less than 75 meters per second (fig. 6(a)). Similarly, the nodal correction velocity losses for initial SS orbital inclinations of 33.5° and 38.5° are small (figs. 6(b) and (c), respectively). From the relatively small nodal correction delta velocity required, the assumption that all nodal correction will be done during the outbound burn and the retroburn seems to be a good one. Any increase in payload resulting from introducing an additional nodal correction burn would be small. Also, engine startup and shutdown losses associated with a very short burn may substantially reduce or completely eliminate the payload gain associated with the added nodal correction burn.

As mentioned earlier, Tug payload capability (fig. 5) is symmetric about a DLA of 0°. Based on this symmetry, maximum Tug payload capability is given in figure 7. The result shown is obtained by departing from the initial SS orbit near the ascending node for positive DLA's and near the descending node for negative DLA's. Maximum Tug payload capability decreases as initial orbital inclination is increased even though total nodal shift decreases.

In figure 8, Tug payload capability is given as a function of initial SS orbital inclination for DLA's of 0°, 10°, 20°, and 30°. Payload capability decreases as initial orbital inclination is increased to approximately 45°, then increases with increasing inclination. Maximum payload capability occurs at an initial SS orbital inclination of 90°. At this point, nodal shift is zero and the trajectory solution becomes planar (no change in inclination). Also, payload and velocity losses remain constant as DLA varies for this orbital inclination. Based on Tug performance and mission requirement, the best SS orbital inclination would be 90°. However, SS payload capability falls off rapidly as orbital inclination is increased to 90°. Also, the allowed launch azimuth range from the

Eastern Test Range limits SS orbital inclinations to less than 56°. With this SS constraint in mind, for low-DLA missions (DLA range, -30° to $+30^{\circ}$), maximum payload can be delivered by departing from a 28.5° inclined orbit. Therefore, this initial orbital inclination was selected to investigate the effects of payload-separation coast time, total trip time, and engine thrust on payload capability.

The effect of payload-separation coast time on payload is shown in figure 9. As expected, payload decreases as the coast time increases. It is well known that energy-change maneuvers can be accomplished most efficiently during high-velocity portions of orbits. During payload-separation coast, as radius increases velocity decreases and the retroburn becomes less efficient. Therefore, the coast phase should be kept as short as possible. The duration of this coast phase (assumed to be 10 min for the baseline case) will be determined by the time required to physically separate the spacecraft and turn the Tug around for proper orientation to perform the retroburn. Engine exhaust impingement on the spacecraft is also a concern during retroburn since the Tug is thrusting essentially opposite to the velocity vector and toward the spacecraft. Thus, sufficient coast time must be allowed for a safe separation distance to be achieved.

Effects of total trip time on Tug payload capability are presented in figure 10. The total-trip-time constraint is satisfied by varying the retroburn. As total trip time is allowed to increase, the amount of energy that must be removed to return the Tug decreases and the payload capability increases. However, the amount of nodal shift increases as total trip time is increased (eq. (1)), which results in a reduction in payload. Therefore, there exists an optimum trip time that gives a maximum payload. Optimum trip time for the mission considered varies between 21 and 26 hours in the declination range of -30° to 30°.

Figure 11 shows the effect of Tug thrust level on payload capability for a range of declinations. As is expected, the payload asymptotically increases to some maximum value as initial thrust increases. These curves were derived by assuming that engine weight remains constant as its thrust level varies. In reality as thrust increases, engine weight increases; and as thrust decreases, so does engine weight. The baseline Tug configuration has an initial thrust of 66 723 newtons. For higher initial thrust, engine weight and consequently Tug hardware weight should increase, decreasing the indicated payload capability. Based on similar arguments for lower thrust, the indicated payload capability should increase. Therefore, there would be a thrust level that gives maximum payload.

SUMMARY OF RESULTS

In this report, mathematical equations were derived to obtain the maximum payload capability of a reusable Tug for planetary missions, taking into account the nodal shift of

the initial Space Shuttle (SS) orbit. The analysis assumes that all nodal corrections will be done during the outbound burn and the retroburn. The sample case analyzed is an inner-planet mission (mission energy, 12 km^2/sec^2). The maximum performance of a typical cryogenic Tug is shown to be 4790 kilograms for declinations of the outgoing asymptote (DLA) between -30^o and 30^o. It is obtained by departing from a 28.5^o SS orbital inclination. Performance varies with DLA; the variation, however, is less than 100 kilograms for the given range of DLA's. Declinations outside the preceding range can be obtained by injecting the Tug into higher inclination orbits with small performance loss.

The velocity loss due to nodal shift is small for departure from a 28.5^o inclined orbit, less than 75 meters per second for declinations between -30^o and 30^o. The corresponding payload loss is a maximum of about 170 kilograms.

The total trip time, the elapsed time from Tug departure to return to the SS, that gives maximum payload varies from 21 to 26 hours as DLA increases from 0^o to 30^o.

Payload-separation coast time was varied from 2 to 20 minutes. Payload decreases almost linearly as coast time increases; therefore, to obtain maximum payload, the separation coast time should be kept as short as possible.

Payload is shown to increase with increasing Tug thrust for a fixed engine weight. However, engine weight increases with increasing thrust, which would reduce the payload gain obtained. Consequently, in the real case, there would be an optimal thrust level.

Lewis Research Center,
National Aeronautics and Space Administration,
Cleveland, Ohio, Oct. 16, 1975,
491-62.

APPENDIX A

SYMBOLS

a_i time at beginning of phase i, sec

b_i time at end of phase i, sec

$\bar{C}$ defined by eq. (18), kg-sec

DLA declination of outgoing asymptote, deg

E energy, m^2/sec^2

e eccentricity

$\hat{f}$ unit thrust direction

G gravitational constant of Earth, m^2/sec^2

H Hamiltonian, kg

H^* augmented Hamiltonian, kg

h angular momentum, m^2/sec^2

$\hat{h}_o$ angular momentum vector of return orbit

i inclination, rad

J oblateness parameter (1.624×10^{-3})

K kappa function, defined by eq. (13), sec

l right-handed Cartesian coordinate system components (l_1 points to initial SS orbital ascending node and l_3 to North Pole)

m mass, kg

P orbital period, sec

p semilatus rectum, m

q constraint

R_E radius of Earth (6.37816×10^6 m)

r radius, m

sign sign function

T return time, sec

T_D trip time, sec

t time, sec

t_p time from perigee, sec

Δt payload-separation coast time, sec

u argument of latitude, rad

V velocity, m/sec

$\hat{V}_\infty$ direction of outgoing asymptote

ΔV_a apogee delta velocity, m/sec

ΔV_p perigee delta velocity, m/sec

ΔV_T total delta velocity ($\Delta V_T = \Delta V_a + \Delta V_p$), m/sec

X defined by eq. (24), kg-sec^2/m

y dummy variable

α angle defined by eq. (D2c), rad

β mass flow rate, kg/sec

γ adjoint multiplier associated with thrust direction, kg

δ yaw attitude, rad

ϵ arbitrary multiplier

ζ dummy variable introduced to make Hamiltonian independent of time, sec

η true anomaly, rad

θ defined by eq. (D2b)

λ adjoint multiplier associated with velocity, kg-sec^2/m

μ adjoint variable associated with position, kg-sec/m

σ adjoint multiplier associated with mass, sec

τ adjoint multiplier associated with variable ζ, kg

φ declination, rad

ψ pitch attitude, rad

Ω longitude of line of nodes, rad

ω argument of pericenter, rad

Subscripts:

a apogee

D desired

e exhaust

H hardware

i index

p *perigee*

Superscripts:

– vector

^ unit vector

· time derivative, (d)/dt

APPENDIX B

GRADIENTS OF RETURN TIME

The return time T is defined as the time from the end of retroburn to rendezvous with the Space Shuttle (SS). It is expressed mathematically as

$$T = \frac{1}{2}(P_1 + P_2) - t_p \tag{B1}$$

where P_1 is the period of the intermediate orbit established at the end of retroburn, t_p is the time from pericenter passage at the end of retroburn, and P_2 is the period of the second intermediate orbit from apogee to return orbit. The periods can be written as

$$P_1 = \frac{2\pi}{G^{1/2}}\left(\frac{r_a + r_p}{2}\right)^{3/2} \tag{B2a}$$

$$P_2 = \frac{2\pi}{G^{1/2}}\left(\frac{r_a + r_{p,D}}{2}\right)^{3/2} \tag{B2b}$$

where r_a and r_p are the instantaneous apogee and perigee radii, respectively; and $r_{p,D}$ is the fixed perigee radius of the return orbit.

The gradients of T with respect to vector $\bar{y}$ (where $\bar{y}$ is either $\bar{r}$ or $\bar{V}$) is given by

$$\nabla_{\bar{y}} T = \frac{3\pi}{4G^{1/2}}\left[\left(\sqrt{\frac{r_a + r_p}{2}} + \sqrt{\frac{r_a + r_{p,D}}{2}}\right)\nabla_{\bar{y}} r_a + \sqrt{\frac{r_a + r_p}{2}}\,\nabla_{\bar{y}} r_p\right] - \frac{\partial t_p}{\partial \eta}\nabla_{\bar{y}}\eta \tag{B3}$$

The gradients of r_a and r_p are given by

$$\nabla_{\bar{V}} r_a = \frac{-\bar{h} \times \bar{r} + r_a^2 \bar{V}}{eG} \tag{B4a}$$

$$\nabla_{\bar{r}} r_a = \frac{\frac{\bar{V} \times \bar{h}}{G} - \left(\frac{r_a}{r}\right)^2 \hat{r}}{e} \tag{B4b}$$

$$\nabla_{\bar{V}} r_p = \frac{\bar{h} \times \bar{r} - r_p^2 \bar{V}}{eG} \tag{B4c}$$

$$\nabla_{\bar{r}} r_p = \frac{\frac{\bar{V} \times \bar{h}}{G} - \left(\frac{r_p}{r}\right)^2 \hat{r}}{e} \tag{B4d}$$

The partial derivative of time from the pericenter with respect to true anomaly $\partial t_p / \partial \eta$ is given by

$$\frac{\partial t_p}{\partial \eta} = \frac{r^2}{h} \tag{B5}$$

The gradient of true anomaly can be obtained from

$$\tan \eta = \frac{h(\bar{r} \cdot \bar{V})}{h^2 - Gr} \tag{B6}$$

The gradients are

$$\nabla_{\bar{V}} \eta = \frac{h \cos^2 \eta}{h^2 - Gr} \left[\bar{r} - \frac{h^2 + Gr}{h^2 - Gr} \left(\frac{\bar{r} \cdot \bar{V}}{h} \right) \nabla_{\bar{V}} h \right] \tag{B7a}$$

and

$$\nabla_{\bar{r}} \eta = \frac{h \cos^2 \eta}{h^2 - Gr} \left[\bar{V} - \frac{h^2 + Gr}{h^2 - Gr} \left(\frac{\bar{r} \cdot \bar{V}}{h} \right) \nabla_{\bar{r}} h + \frac{G(\bar{r} \cdot \bar{V})}{h^2 - Gr} \hat{r} \right] \tag{B7b}$$

The gradients of h are given by

$$\nabla_{\bar{V}} h = \hat{h} \times \bar{r} \tag{B8a}$$

and

$$\nabla_{\bar{r}} h = \bar{V} \times \hat{h} \tag{B8b}$$

From these equations the gradients of T with respect to radius and velocity can be computed.

APPENDIX C

GRADIENTS OF TOTAL DELTA-VELOCITY CHANGE

The total impulse delta-velocity change is the sum of the absolute values of apogee and perigee delta-velocity changes; that is,

$$\Delta V_T = |\Delta V_a| + |\Delta V_p| \tag{C1a}$$

where

$$\Delta V_a = \sqrt{\frac{2Gr_{p,D}}{r_a(r_a + r_{p,D})}} - \sqrt{\frac{2Gr_p}{r_a(r_a + r_p)}} \tag{C1b}$$

$$\Delta V_p = \sqrt{\frac{2Gr_a}{r_{p,D}(r_a + r_{p,D})}} - \sqrt{\frac{2Gr_{a,D}}{r_{p,D}(r_{a,D} + r_{p,D})}} \tag{C1c}$$

Again let $\bar{y}$ stand for either radius or velocity; then the gradient of ΔV_T is given by

$$\nabla_{\bar{y}} \Delta V_T = \text{sign}(1, \Delta V_a)\nabla_{\bar{y}} \Delta V_a + \text{sign}(1, \Delta V_p)\nabla_{\bar{y}} \Delta V_p \tag{C2}$$

The gradient of apogee delta velocity is given by

$$\nabla_{\bar{y}} \Delta V_a = -G\sqrt{\frac{r_a(r_a + r_{p,D})}{2Gr_{p,D}}} \frac{r_{p,D}(2r_a + r_{p,D})}{r_a^2(r_a + r_{p,D})^2} \nabla_{\bar{y}} r_a$$

$$-G\sqrt{\frac{r_a(r_a + r_p)}{2Gr_p}} \left[\frac{1}{(r_a + r_p)^2} \nabla_{\bar{y}} r_p - \frac{r_p(2r_a + r_p)}{r_a^2(r_a + r_p)^2} \nabla_{\bar{y}} r_a \right] \tag{C3}$$

Similarly, the gradient of perigee delta velocity is given by

$$\nabla_{\bar{y}} \Delta V_p = G \sqrt{\frac{r_{p,D}(r_a + r_{p,D})}{2Gr_a}} \frac{1}{\left(r_a + r_{p,D}\right)^2} \nabla_{\bar{y}} r_a \tag{C4}$$

Gradients of apogee and perigee radii with respect to radius and velocity are given by equations (B4).

APPENDIX D

GRADIENTS OF DECLINATION

Declination is defined as the angle between the outgoing asymptote and its projection in the equatorial plane. Let $\hat{V}_\infty$ be the direction of the outgoing asymptote and $\hat{l}_3 = (0, 0, 1)$ be a constant vector pointing to the North Pole. Then the declination is given by

$$\sin \varphi = \hat{l}_3 \cdot \hat{V}_\infty \tag{D1}$$

The outgoing asymptote can be expressed as

$$\hat{V}_\infty = \cos \alpha \hat{r} + \sin \alpha \hat{\theta} \tag{D2a}$$

where

$$\hat{\theta} = \hat{h} \times \hat{r} \tag{D2b}$$

and

$$\alpha = \cos^{-1} - \frac{1}{e} - \eta \tag{D2c}$$

where η is the true anomaly and e the eccentricity at injection. Let $\bar{y}$ represent either radius or velocity; then

$$\nabla_{\bar{y}} \varphi = \frac{\cos \alpha}{\cos \varphi} \left[(-\tan \alpha \hat{r} + \hat{\theta}) \cdot \hat{l}_3 \nabla_{\bar{y}} \alpha + \nabla_{\bar{y}} (\hat{l}_3 \cdot \hat{r}) + \tan \alpha \nabla_{\bar{y}} (\hat{l}_3 \cdot \hat{\theta}) \right] \tag{D3}$$

The gradient of α is given by

$$\nabla_{\bar{y}} \alpha = -\nabla_{\bar{y}} \eta - \frac{1}{e \sqrt{e^2 - 1}} \nabla_{\bar{y}} e \tag{D4}$$

Gradients of true anomaly can be computed from equations (B7) and (B8). The gradients of eccentricity are given by

$$\nabla_{\bar{y}} e = \frac{h}{eG^2} (2E \nabla_{\bar{y}} h + h \nabla_{\bar{y}} E) \tag{D5a}$$

The gradients of h are given by equation (B8). The gradients of energy are as follows:

$$\nabla_{\bar{V}} E = \bar{V} \tag{D5b}$$

$$\nabla_{\bar{r}} E = \frac{G}{r^2} \hat{r} \tag{D5c}$$

In order to compute the gradients of declination, it remains to evaluate the gradients of $\hat{l}_3 \cdot \hat{r}$ and $\hat{l}_3 \cdot \hat{\theta}$. This can be done from the following equations:

$$\nabla_{\bar{V}} (\hat{l}_3 \cdot \hat{r}) = \bar{0} \tag{D6a}$$

$$\nabla_{\bar{r}} (\hat{l}_3 \cdot \hat{r}) = \frac{1}{r} \left[\hat{l}_3 - (\hat{l}_3 \cdot \hat{r}) \hat{r} \right] \tag{D6b}$$

$$\nabla_{\bar{V}} (\hat{l}_3 \cdot \hat{\theta}) = \frac{r}{h} \left[\hat{l}_3 - (\hat{l}_3 \cdot \hat{r}) \hat{r} \right] - \frac{\hat{l}_3 \cdot \hat{\theta}}{h} \nabla_{\bar{V}} h \tag{D6c}$$

$$\nabla_{\bar{r}} (\hat{l}_3 \cdot \hat{\theta}) = \left[\frac{2V}{h} (\hat{l}_3 \cdot \hat{V}) - \frac{1}{r} (\hat{l}_3 \cdot \hat{\theta}) \right] \hat{r} \; \frac{V}{h} \left[(\hat{l}_3 \cdot \hat{r}) \hat{V} + (\hat{r} \cdot \hat{V}) \hat{l}_3 + \frac{1}{V} (\hat{l}_3 \cdot \hat{\theta}) \nabla_{\bar{r}} h \right] \tag{D6d}$$

REFERENCES

1. Weyers, Vernon J.; and Teren, Fred: Optimal Round Trip Space Tug Trajectories for Earth Escape Missions. Presented at Am. Inst. Aeron. and Astron. Astrodynamics Specialists Conf., Fort Lauderdale, Fla., Aug. 17-19, 1971.

2. Zimmerman, Arthur V.: Performance of Recoverable Single and Multiple Space Tugs for Missions Beyond Earth Escape. Presented at JANNAF Propulsion Meeting, New Orleans, La., Nov. 27-29, 1972.

3. Wolverston, Raymond W.: Flight Performance Handbook for Orbital Operations. John Wiley & Sons, Inc., 1963.

4. Mangad, M.; and Schwartz, M. D.: Guidance, Flight Mechanics, and Trajectory Optimization. Volume 4: The Calculus of Variations and Modern Applications. NASA CR-1003, 1968.

5. McIntyre, J. E.: Guidance, Flight Mechanics, and Trajectory Optimization. Volume 7: The Pontryagin Maximum Principle. NASA CR-1006, 1968.

6. Spurlock, Omer F.; and Teren, Fred: Optimum Launch Trajectory for the ATS-E Mission. AIAA Paper 70-1051, Aug. 1970.

7. Teren, Fred; and Spurlock, Omer F.: Optimal Three-Dimensional Launch Vehicle Trajectories with Attitude and Attitude Rate Constraints. NASA TN D-5117, 1969.

TABLE I. - CHARACTERISTICS OF

BASELINE TUG

Initial weight (including payload), kg	28 622
Burnout weight, kg	2767
Engine thrust, N	66 723
Engine specific impulse, I_{sp}, sec	460
Performance reserve, percent of I_{sp}	2

TABLE II. - CHARACTERISTICS OF

BASELINE MISSION

Vis-viva energy, km^2/sec^2	12
Range of declinations, deg	-40 to +40
Total Tug trip time, days	1
Payload-separation coast phase, min	10
Initial orbital altitude, km	185

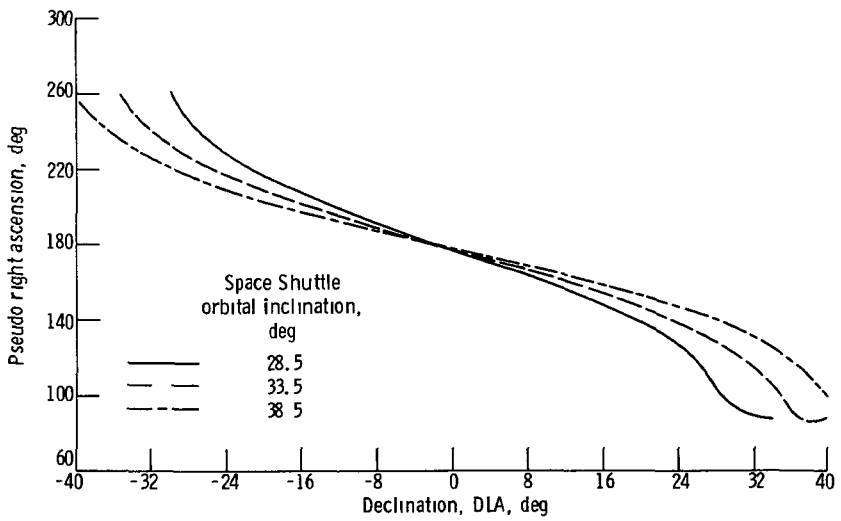

Figure 1 - Pseudo right ascension of outgoing asymptote measured in equatorial plane counterclockwise from ascending node for baseline mission and baseline Tug.

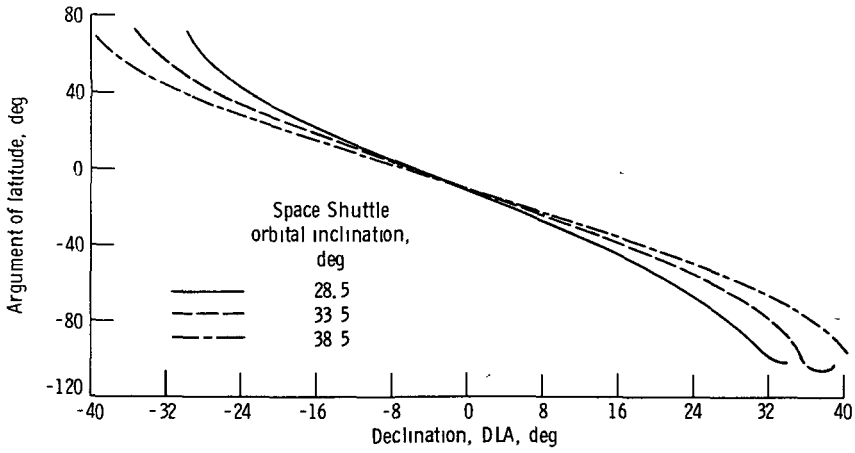

Figure 2 - Tug departure argument of latitude measured from Space Shuttle ascending node for baseline mission and baseline Tug

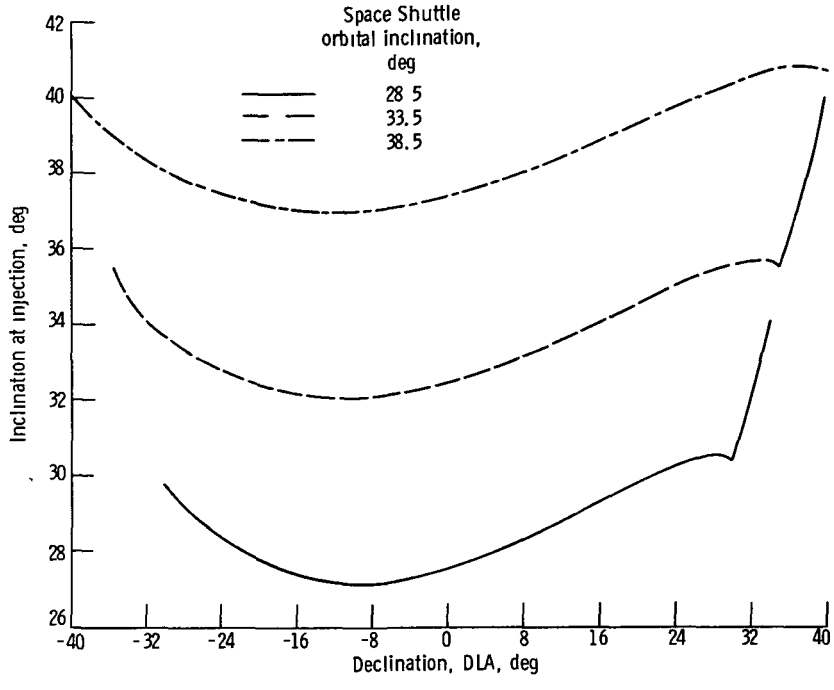

Figure 3 - Inclination of hyperbolic orbit containing desired outgoing asymptote as function of declination for baseline mission and baseline Tug

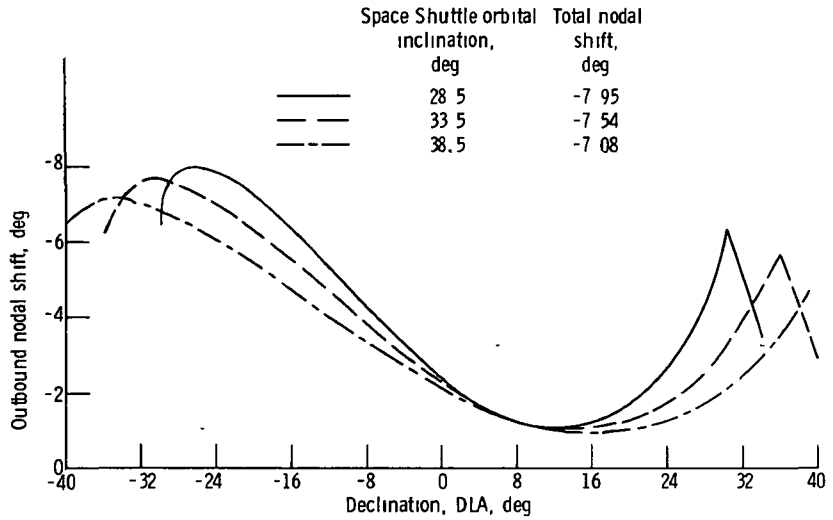

Figure 4 - Nodal shift during outbound burn as function of declination for baseline mission and baseline Tug

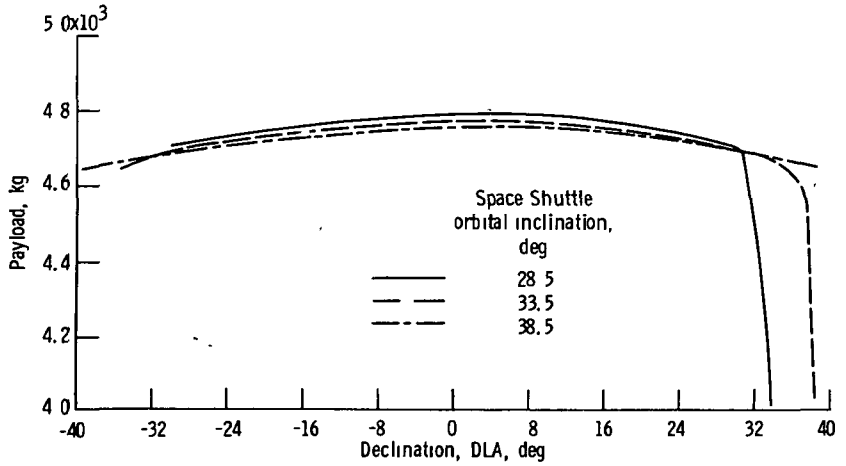

Figure 5. - Tug payload capability as function of declination for baseline mission and baseline Tug.

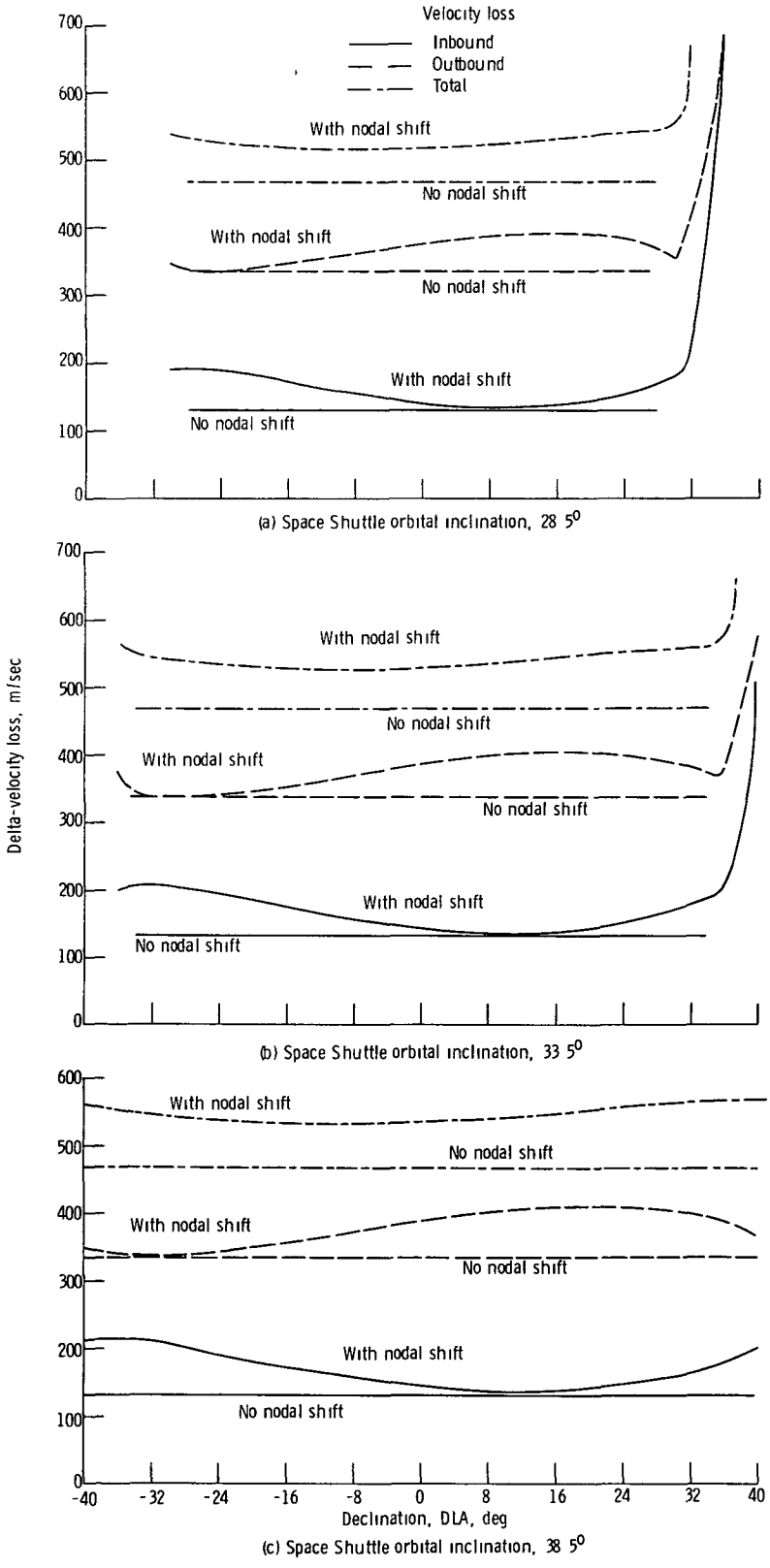

Figure 6 - Velocity loss compared to ideal impulsive orbital transfer on outbound and inbound trajectory legs and to total velocity loss

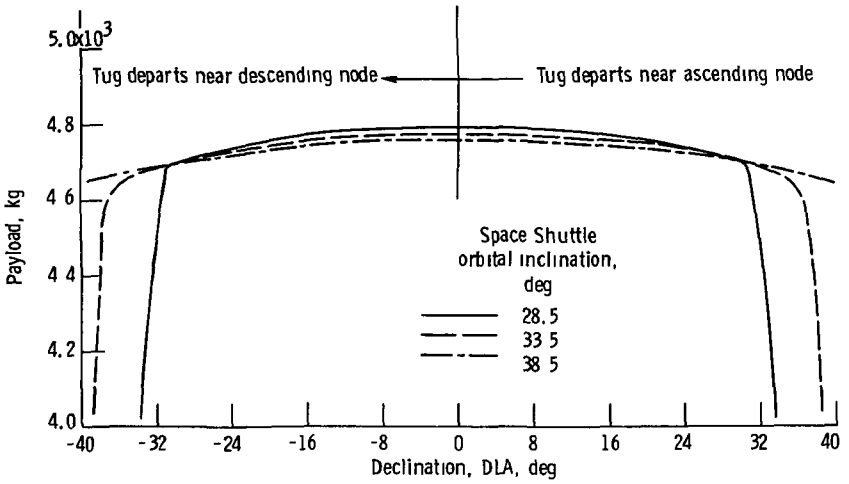

Figure 7 - Maximum tug payload capability as function of declination for baseline mission and baseline Tug.

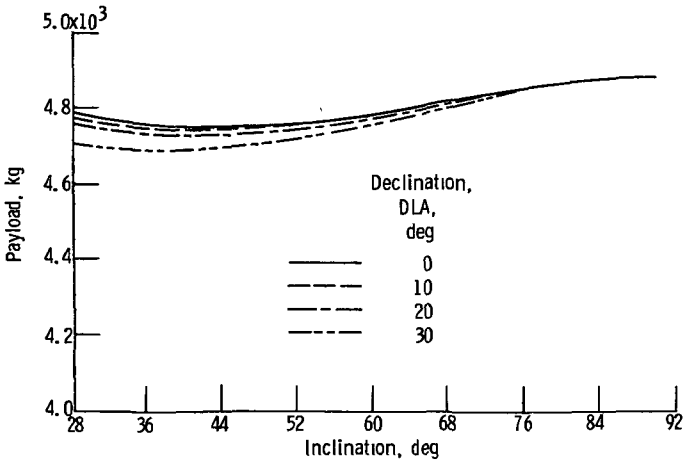

Figure 8. - Tug payload capability as function of Space Shuttle orbital inclination for baseline mission and baseline Tug

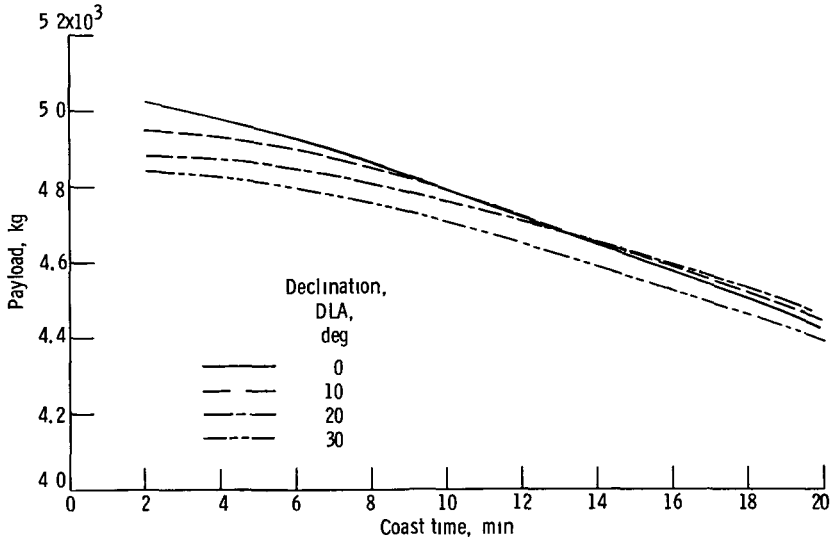

Figure 9 - Tug payload capability as function of separation coast time for baseline Tug departing from 28.5°-inclined Space Shuttle orbit.

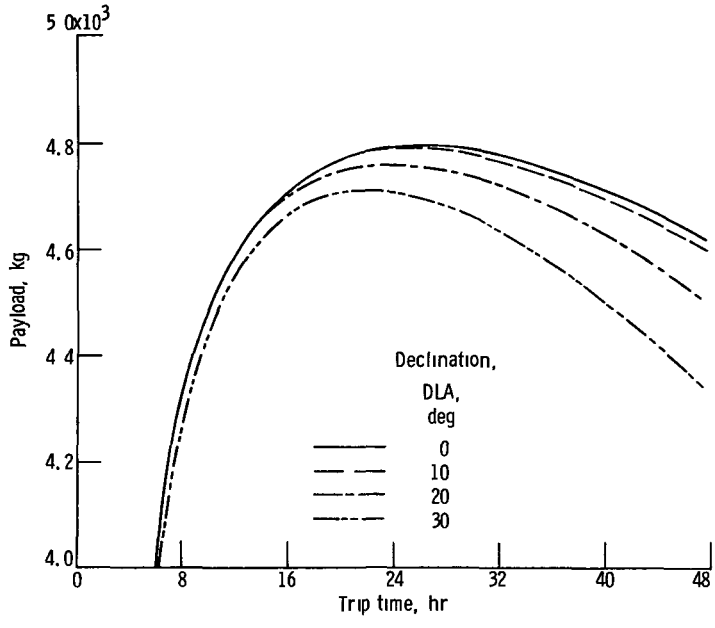

Figure 10. - Tug payload capability as function of total trip time for baseline Tug departing from a 28.5°-inclined Space Shuttle orbit

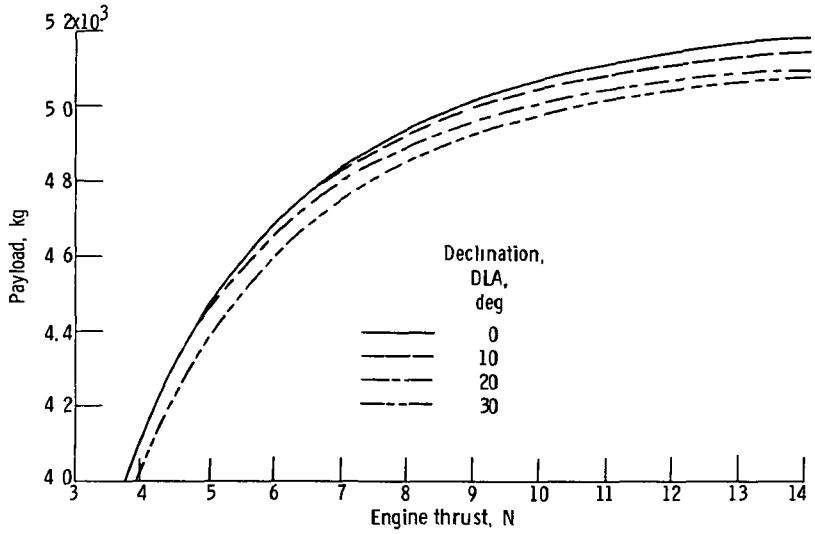

Figure 11. - Tug payload capability as function of Tug engine thrust for constant engine weight, 28.5° Space Shuttle orbital inclination, baseline mission, and baseline Tug.

"The aeronautical and space activities of the United States shall be conducted so as to contribute . to the expansion of human knowledge of phenomena in the atmosphere and space. The Administration shall provide for the widest practicable and appropriate dissemination of information concerning its activities and the results thereof"

—NATIONAL AERONAUTICS AND SPACE ACT OF 1958

NASA SCIENTIFIC AND TECHNICAL PUBLICATIONS

TECHNICAL REPORTS Scientific and technical information considered important, complete, and a lasting contribution to existing knowledge

TECHNICAL NOTES Information less broad in scope but nevertheless of importance as a contribution to existing knowledge

TECHNICAL MEMORANDUMS Information receiving limited distribution because of preliminary data, security classification, or other reasons Also includes conference proceedings with either limited or unlimited distribution.

CONTRACTOR REPORTS Scientific and technical information generated under a NASA contract or grant and considered an important contribution to existing knowledge

TECHNICAL TRANSLATIONS Information published in a foreign language considered to merit NASA distribution in English

SPECIAL PUBLICATIONS Information derived from or of value to NASA activities Publications include final reports of major projects, monographs, data compilations, handbooks, sourcebooks, and special bibliographies

TECHNOLOGY UTILIZATION PUBLICATIONS Information on technology used by NASA that may be of particular interest in commercial and other non-aerospace applications Publications include Tech Briefs, Technology Utilization Reports and Technology Surveys.

Details on the availability of these publications may be obtained from:

SCIENTIFIC AND TECHNICAL INFORMATION OFFICE

NATIONAL AERONAUTICS AND SPACE ADMINISTRATION

Washington, D.C. 20546